Recently Advanced Polymer Materials Containing Dithieno[3,2-*b*:2′,3′-*d*]phosphole Oxide for Efficient Charge Transfer in High-Performance Solar Cells

Kwang Hun Park, Yu Jin Kim, Gi Back Lee, Tae Kyu An, Chan Eon Park, Soon-Ki Kwon,* and Yun-Hi Kim**

Two novel semiconducting polymers based on benzodithiophene and dithienophosphole oxide (DTP) units are designed and synthesized. A novel electron-deficient DTP moiety is developed. Surprisingly, the introduction of DTP units brings highly polarizable characteristics, which is beneficial for the photocurrent in solar cells. Thus, the donor–acceptor type of conjugated polymers based on this novel acceptor has superior charge transfer properties and highly efficient PL quenching efficiencies. As a result, polymer solar cells (PSCs) with high power conversion efficiencies of 6.10% and 7.08% are obtained from poly(3,5-didodecyl-4-phenylphospholo[3,2-b:4,5-b']dithiophene–4-oxide-alt-4,8-bis(5-decylthiophen-2-yl)benzo[1,2-b:4,5-b'] dithiophene) (PDTP–BDTT) and PDTP–4-oxide-alt-4,8-bis(5-decylselenophen-2-yl)benzo[1,2-b:4,5-b']dithiophene) (PDTP–BDTSe), respectively, when the photoactive layer is processed with the 1,8-octanedithiol (ODT) additive. The PDTP–BDTSe copolymer is now the best performing DTP-based material for PSCs. Using the polarizable unit strategy determined in this study for the molecular design of conjugated polymers is expected to greatly advance the development of organic electronic devices.

1. Introduction

Polymer solar cells (PSCs) are a promising technology for low-cost, large-area, and high-throughput energy generation.[1] Bulk-heterojunction (BHJ) blends of conjugated donor polymers and fullerene acceptors now offer power conversion efficiencies (PCEs) of up to 8%–9%.[2] Current efforts are focused on the synthesis of high-performance donor polymers that feature broad absorption spectra, suitable energy levels, and efficient charge transport.[3] A particularly successful approach to the design of new donor polymers with higher efficiencies has been the donor–acceptor approach, in which electron-rich donor monomers are copolymerized with electron-deficient aromatic molecules.[4]

One promising electron-rich donor unit is benzo[1,2-*b*:4,5-*b*′]dithiophene (BDT), which, because of its high degree of planarity, offers enhanced electron delocalization and thus improved charge-carrier mobility.[5] The 2D conjugated BDT unit imparts not only strong interchain properties but also broad light absorption because of its extended side chain. PSCs with BHJs containing BDT donor polymers have been found to show substantially improved PCEs.[6] Among the 2D BDT-based donor materials reported to date, the highest PCE of 9.48% was obtained with a BDT-thienothiophene copolymer with alkylthienyl side chains on the BDT unit.[7]

To develop photovoltaic polymers based on this design, an acceptor unit with relatively strong electron affinity or strong electron-withdrawing capacity is required to lower the bandgap of the resulting polymers. An excellent candidate as a strong acceptor is the dithieno[3,2-*b*:2′,3′-*d*]phosphole oxide (DTP) unit, in which the electronic nature of the phosphole oxide center preferentially exhibits n-type characteristics, leading to a new building block with a higher-lying lowest unoccupied molecular orbital (LUMO) energy level. The highly polarizable nature of the phosphole oxide moiety provides a highly polarized excited state, which significantly improves charge-carrier transfer to a fullerene acceptor and yields a large short-circuit current (J_{SC}).[8] Taking these factors into account, we designed and synthesized two novel copolymers containing BDT and DTP units, designated PDTP–BDTT and PDTP–BDTSe. To our knowledge, there have been no previous reports of the use of

Dr. K. H. Park, Dr. G. B. Lee, Prof. S.-K. Kwon
School of Materials Science & Engineering
and Research Institute for Green Energy
Convergence Technology (RIGET)
Gyeongsang National University
Jin-ju 660-701, South Korea
E-mail: skwon@gnu.ac.kr
Dr. Y. J. Kim, Dr. T. K. An, Prof. C. E. Park
POSTECH Organic Electronics Laboratory
Department of Chemical Engineering
Pohang University of Science and Technology
Pohang 790-784, South Korea
E-mail: cep@postech.ac.kr
Prof. Y.-H. Kim
Department of Chemistry & RIGET
Gyeongsang National University
Jin-ju 660-701, South Korea
E-mail: ykim@gnu.ac.kr

DOI: 10.1002/adfm.201500934

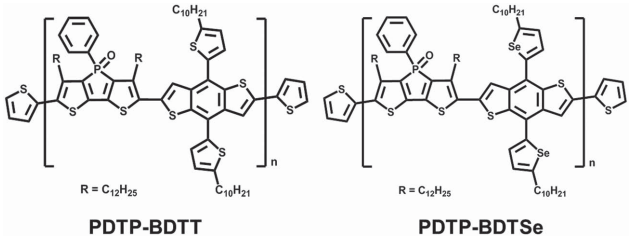

Figure 1. Chemical structures of PDTP–BDTT and PDTP–BDTSe.

copolymers of BDT and DTP in high-performance organic photovoltaic devices.

2. Results and Discussion

The two newly designed polymers, PDTP–BDTT and PDTP–BDTSe, are illustrated in **Figure 1**. These dithienophosphole oxide derivatives had different substituents on the BDT group, i.e., thiophene and selenophene units, respectively. Incorporating selenophene units was expected to enhance the interchain interactions between the polymer chains through strong Se–Se interactions.[9] Two novel DTP-based polymers were synthesized via Stille coupling polymerization using $Pd_2(dba)_3$ and P(*o*-tol)$_3$ as the catalysts and chlorobenzene as the solvent at 110 °C (Supporting Information, Scheme S1). Both copolymers were highly soluble in common organic solvents, such as tetrahydrofuran, chloroform, dichlorobenzene, and chlorobenzene, because of their bulky alkyl side chains. The molecular weight and polydispersity index (PDI) of the synthesized polymers were determined by gel permeation chromatography (GPC) (Supporting Information, Table S1). The number-average molecular weights (M_n) of the PDTP–BDTT and PDTP–BDTSe copolymers were 22 000 and 35 000 g mol^{-1}, and their PDIs were 1.86 and 1.80, respectively. The thermal properties of PDTP–BDTT and PDTP–BDTSe were examined by thermogravimetric analysis (TGA) and differential scanning calorimetry (DSC) under a nitrogen atmosphere. These synthesized polymers showed thermal degradation of only ca. 5 wt% (T_d) above 390°C, indicating that the two polymers were sufficiently thermally stable for use in solar cells.[10] The DSC measurements did not reveal endo or exothermic transitions for either PDTP–BDTT or PDTP–BDTSe between 25 °C and 250 °C (Supporting Information, Table S1 and Figures S1 and S2).

The absorption spectra of the two polymers in chloroform solution and as thin films are shown in **Figure 2**a. The PDTP–BDTT solution exhibited maximum absorption (λ_{max}) at 515 nm while the λ_{max} for PDTP–BDTSe was slightly red-shifted to 524 nm because of the higher intermolecular charge transfer (ICT) transitions derived from the selenophene unit. A more pronounced bathochromic shift and much broader profiles of the extended absorption band were observed for the thin films, and were attributed to stronger intermolecular

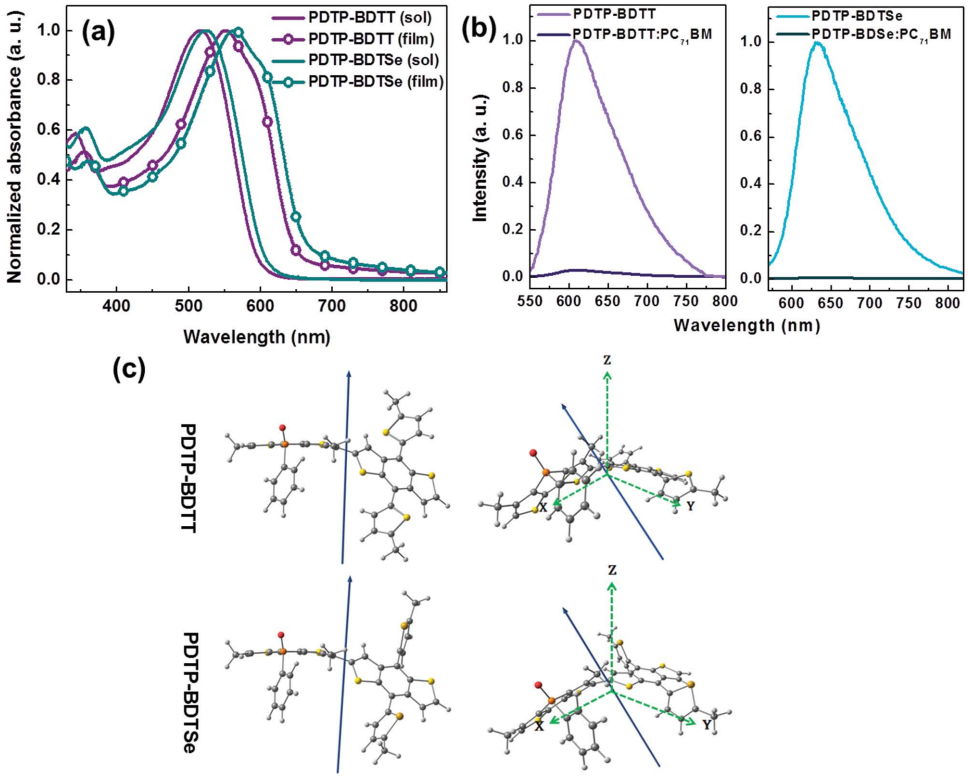

Figure 2. a) Normalized UV–vis absorption spectra of PDTP–BDTT and PDTP–BDTSe. b) Photoluminescence spectra of PDTP–BDTT, PDTP–BDTSe, PDTP–BDTT:PC$_{71}$BM, and PDTP–BDTSe:PC$_{71}$BM. c) Dipole structural calculations for PDTP–BDTT and PDTP–BDTSe. The ground state dipole moments of PDTP–BDTT and PDTP–BDTSe monomer units. The axes (green lines) exhibit the center of mass axes in the X, Y, and Z directions. The vector of the dipole represents the direction of electron flow in these directions.

π–π stacking in the thin films.[11] Notably, the absorption onset of PDTP–BDTSe was red-shifted by ca. 25 nm, corresponding to a lower band gap (E_g^{opt} = 1.80 eV) than PDTP–BDTT (E_g^{opt} = 1.89 eV). These results were consistent with earlier experimental studies and indicated that the replacement of thiophene with selenophene results in a reduction of the optical bandgap because of the increased quinoid character in the polymer chain.[9]

The absorption characteristics of polymer:(6,6)-phenyl-C71-butyric acid methyl ester ($PC_{71}BM$) blended films mixed in a 1:4 weight ratio are shown in Supporting Information, Figure S3, which will implement in the device preparations. As both DTP-based copolymers have low absorption below 450 nm, $PC_{71}BM$ was chosen as the electron acceptor for the photovoltaic cell in order to increase the light absorption between 300 and 450 nm.[12a] Therefore, it can be seen that PDTP–BDTT:$PC_{71}BM$ and PDTP–BDTSe:$PC_{71}BM$ mixtures absorb strongly throughout the range of 300 to 700 nm. The relative absorption spectra in overall UV–vis range is red-shifted under the following sequence: PDTP–BDTT:$PC_{71}BM$ < PDTP–BDTSe:$PC_{71}BM$. These results can be ascribed to the strong intermolecular interaction between polymer and PCBM, respectively, which makes the PDTP-BDTSe and $PC_{71}BM$ domains more ordered.[12b]

Photoluminescence (PL) spectra of spin-cast films of pure PDTP–BDTT and PDTP–BDTSe, and of 1:4 (w/w) blends of the polymers and $PC_{71}BM$, were examined for their charge transfer properties (Figure 2b). PDTP–BDTT showed a strong PL emission band with a maximum at 610 nm, whereas PDTP–BDTSe exhibited a strong emission band at 633 nm, slightly red-shifted compared to that of PDTP–BDTT. Films of the PDTP–BDTT:$PC_{71}BM$ and PDTP–BDTSe:$PC_{71}BM$ blends exhibited an emission band that was almost completely quenched (ca. 98% PL quenching efficiency), indicating effective charge transfer between the polymer and the $PC_{71}BM$ (i.e., more effective dissociation into separate charge carriers). The band for the PDTP–BDTSe:$PC_{71}BM$ blend showed a slightly lower intensity than that for PDTP–BDTT, which suggested that the PDTP–BDTSe polymer dissociated more efficiently into carriers and thereby improved charge transfer to the PCBM.[13]

The dipole moments were calculated for the monomers used to build the PDTP–BDTT and PDTP–BDTSe copolymers to better understand the enhanced charge transfer of the copolymers. The degree of photoinduced charge transfer is related to the ground- and excited-state dipole moments.[14] Dipole analysis for both the ground (μ_g) and excited states (μ_e) was performed at the density functional theory (DFT) level, by the hybrid Becke three-parameter exchange/Lee–Yang–Parr correlation functionals (B3LYP) as implemented in the Gaussian 09W software. The calculated μ_g dipole moments of the PDTP–BDTT and PDTP–BDTSe were 2.48 and 2.93 D, respectively, and μ_e was 4.30 D for PDTP–BDTT and 4.62 D for PDTP–BDTSe. These calculated μ_e dipole moments for the two monomers were higher than that of a BDT-based polymer such as PTB7 (4.07 D for the single repeat unit),[14a] indicating that our BDT-based polymers with the DTP unit had better charge separating abilities. This result also indicated that the polarizable DTP moiety in the BDT-based polymer chain indeed contributed to the very high μ_e values, leading to efficient charge transfer to the PCBM. The μ_e dipole moment for PDTP–BDTSe was 4.62 D, which was higher than that for the PDTP–BDTT monomer. These calculations indicated enhanced charge transfer properties of the PDTP–BDTSe polymer,[14c] which supported the results of PL analysis. The directionality and amplitude of the local dipole moments of the monomers used to synthesize the PDTP–BDTT and PDTP–BDTSe copolymers are shown in Figure 2c; these properties are governed by the phosphole oxide unit.

The electrochemical properties of both conjugated polymers were investigated using cyclic voltammetry (Supporting Information, Figure S5a). The highest occupied molecular orbital/lowest unoccupied molecular orbital (HOMO/LUMO) values for the PDTP–BDTT and PDTP–BDTSe were calculated based on the onset of the oxidation and reduction potentials, respectively, using the known energy level for ferrocene, which is 4.8 eV below the vacuum level.[15] The calculated HOMO and LUMO values for the PDTP–BDTT and PDTP–BDTSe copolymers were –5.58 and –3.66 eV and –5.46 and –3.62 eV, respectively. Both PDTP–BDTT and PDTP–BDTSe had nearly identical HOMO energy levels that ensured a high V_{OC}[16]; the LUMO energy levels about 0.3 eV above the LUMO (–4.00 eV) of the $PC_{71}BM$ n-type acceptor generated a driving force for energetically favorable electron transfer (see Supporting Information, Figure S5b).[17]

The photovoltaic performances of the photovoltaic polymers were characterized as follows. BHJ thin-film solar cells with a conventional structure of indium tin oxide (ITO)/poly(3,4-ethylenedioxythiophene)polystyrene sulfonate (PEDOT:PSS)/polymer:$PC_{71}BM$/Ca/Al were fabricated using PDPT–BDTT and PDTP–BDTSe as electron donors and $PC_{71}BM$ as the electron acceptor. The device efficiency was optimized with respect to 1) the copolymer:$PC_{71}BM$ blend ratio, 2) the active layer thickness, 3) thermal annealing conditions, and 4) the presence of 1,8-octanedithiol (ODT) as a processing additive (see the Supporting Information). Under AM 1.5 G illumination at 100 mW cm^{-2}, the optimized devices fabricated with the PDTP–BDTT and PDTP–BDTSe had superior open-circuit voltages (V_{OC}) and short-circuit current densities (J_{SC}), which resulted in higher PCEs (**Figure 3**a and **Table 1**). The measured V_{OC} followed the HOMO energy levels of the polymers, and were 0.86–0.87 V and 0.84–0.85 V for PDTP–BDTT and PDTP–BDTSe, respectively.[18] When made without the ODT additive, the PDTP–BDTT and PDTP–BDTSe devices had PCEs of only 4.86% and 5.52%, respectively. The higher PCE obtained for the PDTP–BDTSe:$PC_{71}BM$ device was primarily because of the improved J_{SC} value resulting from higher charge generation and more efficient charge transfer, as noted above. The J_{SC} and the fill factor (FF) were significantly improved when the ODT additive was used; the PCEs were 6.10% for PDTP–BDTT and 7.08% for PDTP–BDTSe. The considerable increase in PCE mainly stemmed from the improved J_{SC} and FF.

The J_{SC} and FF depend strongly on film morphology, nanostructural order, and charge carrier mobility. The J_{SC} is strongly related to the photoresponse (conversion of input photons to photocurrent). The photoresponse of the solar cell based on PDTP–BDTSe:$PC_{71}BM$ exceeded 72%, whereas that of the PDTP–BDTT:$PC_{71}BM$ device exceeded 67% (Figure 3b). Similar behavior was observed for the BHJ solar cell processed

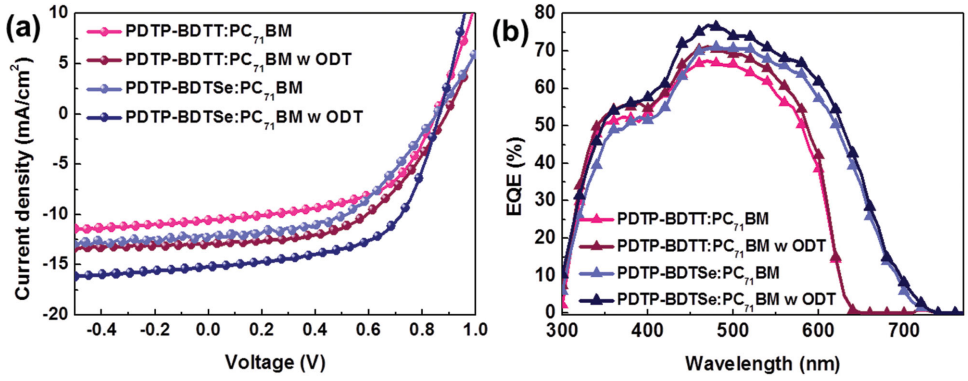

Figure 3. Characteristics a) *J–V* plots and b) EQE spectra of BHJ solar cells based on the PDTP–BDTT:$PC_{71}BM$ and PDTP–BDTSe:$PC_{71}BM$ composite films.

using ODT. The higher external quantum efficiency (EQE) of the copolymer:$PC_{71}BM$ cells made with the ODT additive was attributed to a greater conversion of input photons to photocurrent at all absorption wavelengths, consistent with the observed higher circuit current.[19]

Polymer:$PC_{71}BM$ blend films were analyzed by atomic force microscopy (AFM) and 2D grazing-incidence X-ray diffraction (2D-GIXD) to correlate organic photovoltaic (OPV) cell performance with nanostructural order and morphology. **Figure 4**a shows that cast films of PDTP–BDTT:$PC_{71}BM$ and PDTP–BDTSe:$PC_{71}BM$ prepared at a blend ratio of 1:4 had slightly smaller root-mean square (RMS) roughnesses (RMS = 0.98 nm for PDTP–BDTT and 1.13 nm for PDTP–BDTSe) and homogeneously flat surface morphologies. However, use of the ODT processing additive caused the formation of more aggregated domains and phase-separated morphologies in these films. Furthermore, both blend films made with ODT were rougher, i.e., RMS = 2.27 and 4.34 nm for PDTP–BDTT and PDTP–BDTSe, respectively. The aggregated domains were probably due to enhanced intermolecular interactions between the polymer chains.[18a] Surface roughness also indicates the degree of self-organization of a polymer.[18b] The increase in surface roughness and more ordered crystalline domains may effectively provide separate pathways for electrons and holes, and thereby increase the J_{SC}.[20] The 2D-GIXD results shown in Figure 4b support the morphological observations. Both pristine polymer:$PC_{71}BM$ thin films only showed weak isotropic scattering rings at q_z = 1.32 Å^{-1}, which were characteristic of randomly oriented $PC_{71}BM$ on the substrate.[21] However, when 0.5% ODT was added, a strong reflection peak at q_z = 0.261 Å^{-1} was observed for the PDTP–BDTT:$PC_{71}BM$ blend film, which suggested improved order in the PDTP–BDTT crystallites.[22] Similarly, for the PDTP–BDTSe:$PC_{71}BM$ film processed with ODT, there was a broad reflection in the out-of-plane and in-plane directions of the 2D-GIXD pattern at q = 0.273 Å^{-1}, which also indicated that the crystallinity of the PDTP–BDTSe random copolymer had improved.[22] Thus, ODT as an additive improved the ordered packing of the PDTP–BDTT and PDTP–BDTSe polymer chains, which served to significantly improve the J_{SC} and the PCE of devices made with them.[22] This change in nanostructural order with the ODT additive was consistent with previous studies concerning several other high-performance polymer systems, such as the BDT-based polymer series.[23]

Table 1. Photovoltaic performances of the DTP-based polymer:$PC_{71}BM$ BHJ devices.

Polymer	Conditions	V_{oc} [V]	J_{sc} [mA cm^{-2}]	FF [%]	PCE^{max} [%]	PCE^{avg}[a)] [%]
PDTP–BDTT	as-cast	0.86	11.6	48.8	4.86	4.72
	ODT 0.5 vol%	0.87	13.2	53.1	6.10	5.98
PDTP–BDTSe	as-cast	0.84	12.9	51.0	5.52	5.40
	ODT 0.5 vol%	0.85	14.8	56.3	7.08	6.89

[a)]PCE^{avg} : Data obtained from eight devices.

Carrier mobility was measured to quantitatively investigate the effects of interchain packing on the charge transport property; the space charge limit current (SCLC) method was used. The charge carrier mobility was measured in the dark using hole-only devices (ITO/PEDOT:PSS/polymer or polymer:$PC_{71}BM$/Au) and electron-only devices (Al/polymer:$PC_{71}BM$/Al) and was determined from the slope of the plot of log J_D versus voltage (see **Figure 5** and Supporting Information, Figure S10). The hole mobility of PDTP–BDTSe (1.02×10^{-3} cm^2 V^{-1} s^{-1}) was higher than that of PDTP–BDTT (8.79×10^{-4} cm^2 V^{-1} s^{-1}). This enhanced hole mobility was attributed to the denser packing of the polymers containing selenophene units,[24] consistent with the results of UV analysis of pure polymer films. Higher hole mobility was also observed for the PDTP–BDTSe:$PC_{71}BM$ blends compared with the PDTP–BDTT:$PC_{71}BM$ blends, i.e., 8.91×10^{-5} versus 2.53×10^{-4} cm^2 V^{-1} s^{-1}. This also suggested that it was the stronger intermolecular interactions of PDTP–BDTSe that enabled the observed higher hole mobility in the BHJ films.[25] These trends appear in the electron mobility results. The electron mobility of the PDTP–BDTSe:$PC_{71}BM$ film (1.15×10^{-5} cm^2 V^{-1} s^{-1}) is quite higher than those of PDTP–BDTT:$PC_{71}BM$ (2.73×10^{-6} cm^2 V^{-1} s^{-1}). The higher carrier mobility permitted charge carriers to travel faster during the charge transport process and diminished the recombination of excitons, resulting in a high current density and FF.[25,26] It was noteworthy that both blend films processed with ODT had higher carrier mobilities

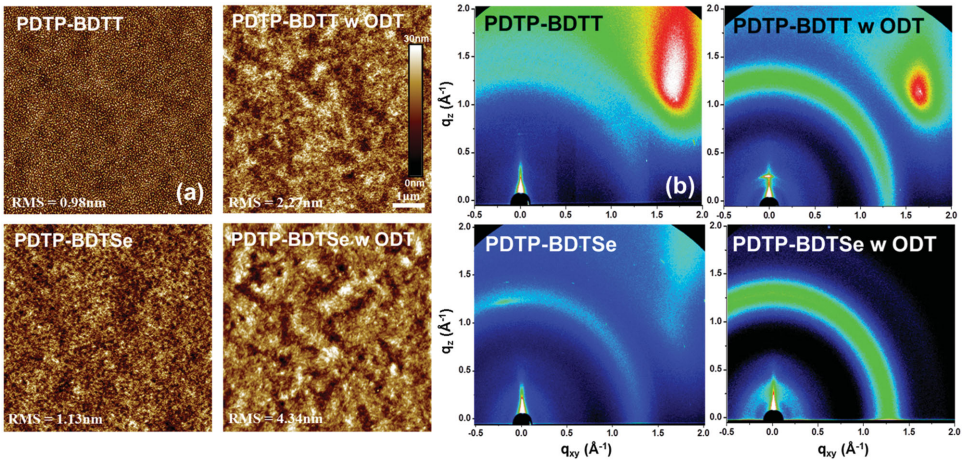

Figure 4. Characterization of active layer blend films through: a) atomic force microscopy (AFM, height images) and b) 2D grazing incidence X-ray diffraction (GIXD).

than PDTP–BDTT:$PC_{71}BM$ and PDTP–BDTSe:$PC_{71}BM$ films cast without the additive. It is likely that the ODT improved molecular packing, as indicated by the AFM and 2D-GIXD studies, which resulted in increased carrier mobility.

3. Conclusion

In summary, two novel copolymers containing BDT and DTP units were synthesized. A novel electron-deficient DTP moiety was developed. The donor–acceptor type of conjugated polymers based on this novel acceptor had superior charge transfer properties and highly efficient PL quenching efficiencies. Polymer solar cells with high PCEs of 6.10% and 7.08% were obtained from PDTP–BDTT and PDTP–BDTSe, respectively, when the photoactive layer was processed with the ODT additive. The PDTP–BDTSe copolymer is now the best performing DTP-based material for PSCs. Using the polarizable unit strategy determined in this study for the molecular design of conjugated polymers is expected to greatly advance the development of organic electronic devices.

4. Experimental Section

Materials and Synthesis of Polymers: The detailed procedures and materials for synthesis of two polymers were described in the Supporting Information.

General Characterization: ^{1}H-NMR spectra were acquired from a Bruker AM-200 spectrometer. ^{13}C-NMR spectra were measured on a Bruker Advance-300 spectrometer. HRMS (EI) spectra were recorded on a high resolution GC mass spectrometer with LabRAM HR800 UV. Fourier transform infrared spectroscopy (FT-IR) was performed on a NICOLET 6700 (Thermo electron corporation). Mass (MALDI-TOF/TOF) spectra were determined on a High resolution 4800 Tof/Tof mass spectrometer with Voyager DE-STR. The number-average (M_n) molecular weights were measured by GPC using the Shimadzu LG solution, chlorobenzene as the eluent with a flow rate of 1.0 mL min^{-1}, and polystyrenes as standard to calibrate. The thermal analysis (TGA) were performed on a TA TGA 2100 thermogravimetric analyzer under a purified nitrogen with a heating rate of 10 °C min^{-1}. DSC was conducted under nitrogen on a TA Instruments 2100 DSC. The sample was heated with 10 °C min^{-1} from 25 to 250 °C. UV–vis absorption spectra were determined using a Carry 5000 UV–vis-near-IR double beam spectrophotometer. PL spectra were obtained using a FP-6500 (JASCO). Cyclic voltammetry (CV) was performed using a PowerLab/AD instrument model system in 0.1 M solution of tetrabutylammonium hexafluorophospate (Bu_4NPF_6) in anhydrous acetonitrile as supporting electrolyte at a scan rate of

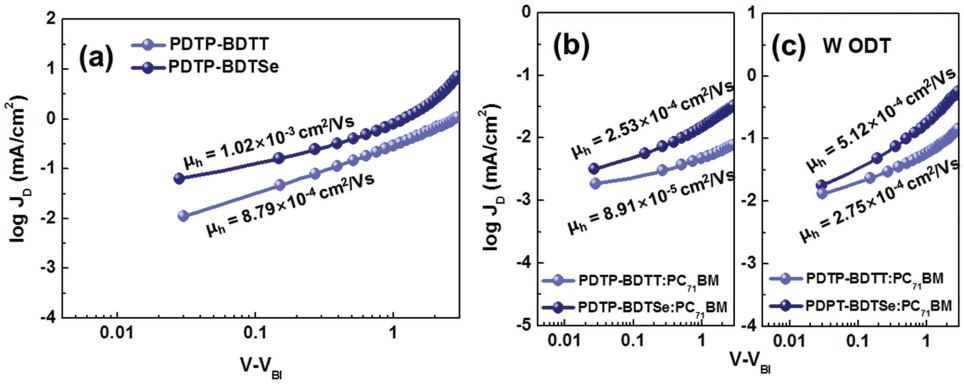

Figure 5. Current–voltage (*J*–*V*) characteristics of hole only devices for a) pure two polymers, b) polymer:$PC_{71}BM$ blends, and c) blend films processed with ODT additive in the dark.

50 mV s^{-1}. A glassy carbon disk (≈0.05 cm^2) coated with a thin polymer film, an Ag/AgCl electrode, and a platinum wire were used as working electrode, reference electrode, and counter electrode, respectively. DFT calculations were carried out at the B3LYP/6-31G* level of theory using the Gaussian 09W computational programs.

Fabrication and Characterization of Photovoltaic Cells: PDTP–BDTT:$PC_{71}BM$ and PDTP–BDTSe:$PC_{71}BM$ devices were fabricated on an ITO-coated glass substrate with the following conventional structure: ITO-coated glass substrate/PEDOT:PSS/Polymer:$PC_{71}BM$/Ca/Al. The ITO-coated glass substrate was first cleaned via successive sonication in detergent, deionized water, acetone, and isopropyl alcohol, with subsequent UV-Ozone treatment of the samples for 30 min. PEDOT:PSS (Baytron P VP AI 4083, filtered at 0.45 μm polyvinylidene difluoride (PVDF)) was spin-cast from an aqueous solution to form a film of ca. 40 nm thickness. The substrate was dried for 10 min at 120 °C in air and then transferred into a glove box to spin-cast the active layer. Subsequently, the polymer:$PC_{71}BM$ active layer was spin-coated on the PEDOT:PSS layer from the donor–acceptor blend solutions in different ratios, thickness, thermal treatment, and processing ODT additive. Solutions containing a mixture of the polymer and $PC_{71}BM$ in dichlorobenzene at a concentration of 40 mg mL^{-1} were prepared and then filtered through a 0.2 polytetrafluoroethylene (PTFE) filter prior to use. At the final stage, a 2 nm thick Ca topped with aluminum (Al, 100 nm) electrode was deposited by thermal evaporation under vacuum at 2×10^{-6} Torr. The current density–voltage (*J*–*V*) characteristics of the photovoltaic devices were recorded from a Keithley Model 2400 Source Meter under ambient conditions using. An Oriel xenon lamp (450 W) with an AM 1.5 G filter was used as the solar simulator. The light intensity was calibrated to 100 mW cm^{-2} using a calibrated silicon cell with a KG5 filter, which is traced to the National Renewable Energy Laboratory (LREL). The active area was 0.09 cm^2 and measurements were carried out through a shadow mask under an ambient atmosphere. EQE spectra were characterized using a photomodulation spectroscopic set-up (model Merlin, Oriel) with a calibrated Si UV detector and a SR570 low noise current amplifier.

AFM and GIXD Measurements: The topographic images (surface area: 5 μm × 5 μm) of the active blend films were taken by using AFM (Multimode IIIa, Digital Instruments) in tapping mode under ambient conditions. 2D-GIXD specular scans were recorded for structural analysis using the 9A beam line at the Pohang Acceleration Laboratory. The 2D-GIXD measurements were carried out with a sample-to-detector distance of 209.761 mm. Data were typically recorded for ten seconds using an X-ray radiation source of λ = 1.1189 nm with a 2D charge-coupled detector (CCD) (Roper Scientific, Trenton, NJ, USA). The samples were mounted on a home-built z-axis goniometer equipped with a vacuum (<10^{-3} Torr) chamber. The incidence angle a_i for the X-ray beam was set to 0.12° (a fixed incident angle), which was intermediate between the critical angles of the films and the substrate ($a_{c,f}$ and $a_{c,s}$). Samples for the X-ray measurements were prepared by spin-coating the polymer:$PC_{71}BM$ solution on the PEDOT:PSS spin-coated ITO glass.

SCLC Measurements: The hole only devices were fabricated with the configuration of ITO/PEDOT:PSS/polymer or polymer:$PC_{71}BM$/Au. The active layer was spin-coated on the PEDOT:PSS layer to same method with photovoltaic device fabrications. The Au layer was deposited under a low speed (1 Å s^{-1}) to avoid the penetration of Au atoms into the active layer. Electron-only devices (a Al/polymer:$PC_{71}BM$/Al architecture) were fabricated by the following procedure. A thick Al layer (70 nm), which acted as the anode, was vacuum-deposited on a glass substrate. Sequentially, a polymer:$PC_{71}BM$ blend layer were spin-coated onto Al anode electrode. An upper Al (100 nm) layer was then vaccum-deposited as the cathode. Mobilities were extracted by fitting the current-voltage curves using the Mott–Curney relationship (space charge limited current)

$$J = \frac{9}{8}\varepsilon_0\varepsilon_r\mu_h\frac{V^2}{L^3}$$

where *J* is the current density, *L* is the film thickness of active layer, μ_h is the hole mobility, ε_r is the relative dielectric constant of the transport medium, ε_0 is the permittivity of free space, *V* is the internal voltage in the device and $V = V_{appl} - V_r - V_{bi}$, where V_{appl} is the applied voltage to the device, V_r is the voltage drop due to contact resistance and series resistance across the electrodes, and V_{bi} is the built-in voltage due to the relative work function difference of the two electrodes. The V_{bi} can be determined from the transition between the Ohmic region and the SCLC region.

Supporting Information

Supporting Information is available from the Wiley Online Library or from the author.

Acknowledgements

K.H.P. and Y.J.K. contributed equally to this work. This study was supported by a grant (2011-0031639 and 2012M3A6A55225) from the Center for Advanced Soft Electronics under the Global Frontier Research Program of the Ministry of Education, Science and Technology and by a grant from the National Research Foundation of Korea (NRF), funded by the Korean Government (2012R1A2A2A06047047 and NRF-2014R1A2A1A05004993).

Received: March 9, 2015
Revised: May 3, 2015
Published online: May 26, 2015

[1] a) G. Yu, J. Gao, J. C. Hummelen, F. Wudl, A. J. Heeger, *Science* **1995**, *270*, 1789; b) S. Günes, H. Neugebauer, N. S. Sariciftci, *Chem. Rev.* **2007**, *107*, 1324; c) G. Li, Y. Yang, *Nat. Photonics* **2012**, *6*, 153.

[2] a) J. You, L. Dou, K. Yoshimura, T. Kato, K. Ohya, T. Moriarty, K. Emery, C.-C. Chen, J. Gao, G. Li, Y. Yang, *Nat. Commun.* **2013**, *4*, 1446; b) K. H. Hendriks, G. H. L. Heintges, V. S. Gevaerts, M. M. Wienk, R. A. J. Janssen, *Angew. Chem. Int. Ed.* **2013**, *52*, 8341.

[3] a) Z. C. He, C. M. Zhong, S. J. Su, M. Xu, H. B. Wu, Y. Cao, *Nat. Photonics* **2012**, *6*, 591; b) Y. Li, *Acc. Chem. Res.* **2012**, *45*, 723; c) P. M. Beaujuge, J. M. J. Fréchet, *J. Am. Chem. Soc.* **2011**, *133*, 20009; d) J.-S. Wu, S.-W. Cheng, Y.-J. Cheng, C.-S. Hsu, *Chem. Soc. Rev.* **2015**, *44*, 1113; e) H. Zhou, L. Yang, W. You, *Macromolecules* **2012**, *45*, 607.

[4] a) Y. Sun, J. Seifter, M. Wang, L. A. Perez, C. Luo, G. C. Bazan, F. Huang, Y. Cao, A. J. Heeger, *Adv. Energy Mater.* **2014**, *4*, 1301601; b) B. Walker, J. Liu, C. Kim, G. C. Welch, J. K. Park, J. Lin, P. Zalar, C. M. Proctor, J. H. Seo, G. C. Bazan, T.-Q. Nguyen, *Energy Environ. Sci.* **2013**, *6*, 952.

[5] a) J. Yuan, H. Dong, M. Li, X. Huang, J. Zhong, Y. Li, W. Ma, *Adv. Mater.* **2014**, *26*, 3624; b) M. Zhang, X. Guo, W. Ma, S. Zhang, L. Huo, H. Ade, J. Hou, *Adv. Mater.* **2014**, *26*, 2089; c) T. Xu, L. Yu, *Mater.Today* **2014**, *17*, 11.

[6] a) J. Gao, L. Dou, W. Chen, C.-C. Chen, X. Guo, J. You, B. Bob, W.-H.Chang, J. Strzalka, C. Wang, G. Li, Y. Yang, *Adv. Energy Mater.* **2014**, *4*, 1300739; b) Y. Dong, X. Hu, C. Duan, P. Liu, S. Liu, L. Lan, D. Chen, L. Ying, S. Su, X. Gong, F. Huang, Y. Cao, *Adv. Mater.* **2013**, *25*, 3683.

[7] L. Ye, S. Zhang, W. Zhao, H. Yao, J. Hou, *Chem. Mater.* **2014**, *26*, 3603.

[8] a) Y. Matano, H. Ohkubo, T. Miyata, Y. Watanabe, Y. Hayashi, T. Umeyama, H. Imahori, *Eur. J. Inorg. Chem.* **2014**, *2014*, 1620; b) R. A. Kruger, T. J. Gordon, T. C. Sutherland, T. Baumgartner, *J. Polym. Sci. Part A:Polym. Chem.* **2011**, *49*, 1201.

[9] a) I. Kang, H.-J. Yun, D. S. Chung, S.-K. Kwon, Y.-H. Kim, *J. Am. Chem. Soc.* **2013**, *135*, 14896; b) I. Kang, T. K. An, J. Hong, H.-J. Yun, R. Kim, D. S. Chung, C. E. Park, Y.-H. Kim, S.-K. Kwon, *Adv. Mater.*

2013, *25*, 524; c) D. H. Wang, A. Pron, M. Leclerc, A. J. Heeger, *Adv. Funct. Mater.* **2013**, *23*, 1297.
[10] C. Cui, W.-Y. Wong, Y. Li, *Energy Environ. Sci.* **2014**, *7*, 2276.
[11] J. Jo, A. Pron, P. Berrouard, W. L. Leong, J. D. Yuen, J. S. Moon, M. Leclerc, A. J. Heeger, *Adv. Energy Mater.* **2012**, *2*, 1397.
[12] a) Y. Zou, A. Najari, P. Berrouard, S. Beaupré, B. R. Aich, Y. Tao, M. Leclerc, *J. Am. Chem. Soc.* **2010**, *132*, 5230; b) B. Walker, A. B. Tamayo, X.-D. Dang, P. Zalar, J. H. Seo, A. Garcia, M. Tantiwiwat, T.-Q. Nguyen, *Adv. Funct. Mater.* **2009**, *19*, 3063.
[13] Z. Ma, D. Dang, Z. Tang, D. Gedefaw, J. Bergqvist, W. Zhu, W. Mammo, M. R. Andersson, O. Inganas, F. Zhang, E. Wang, *Adv. Energy Mater.* **2014**, *4*, 1301455.
[14] a) B. Carsten, J. M. Szarko, H. J. Son, W. Wang, L. Lu, F. He, B. S. Rolczynski, S. J. Lou, L. X. Chen, L. Yu, *J. Am. Chem. Soc.* **2011**, *133*, 20468; b) T. Xu, L. Lu, T. Zheng, J. M. Szarko, A. Schneider, L. X. Chen, L. Yu, *Adv. Funct. Mater.* **2014**, *24*, 3432; c) J. W. Jo, S. Bae, F. Liu, T. P. Russell, W. H. Jo, *Adv. Funct. Mater.* **2015**, *25,* 120 .
[15] Y. Zang, C.-Z. Li, C.-C. Chueh, S. T. Williams, W. Jiang, Z.-H. Wang, J.-S. Yu, A. K.-Y. Jen, *Adv. Mater.* **2014**, *26*, 5708.
[16] J. Yuan, Z. Zhai, H. Dong, J. Li, Z. Jiang, Y. Li, W. Ma, *Adv. Funct. Mater.* **2013**, *23*, 885.
[17] S.-W. Tsang, S. Chen, F. So, *Adv. Mater.* **2013**, *25*, 2434.
[18] M. C. Scharber, D. Mühlbacher, M. Koppe, P. Denk, C. Waldauf, A. J. Heeger, C. J. Brabec, *Adv. Mater.* **2006**, *18*, 789.
[19] X. Guo, N. Zhou, S. J. Lou, J. Smith, D. B. Tice, J. W. Hennek, R. P. Ortiz, J. T. L. Navarrete, S. Li, J. Strzalka, L. X. Chen, R. P. H. Chang, A. Facchetti, T. J. Marks, *Nat. Photonics* **2013**, *7*, 825.
[20] a) H. Zhou, Y. Zhang, J. Seifter, S. D. Collins, C. Luo, G. C. Bazan, T.-Q. Nguyen, A. J. Heeger, *Adv. Mater.* **2013**, *25*, 1646; b) Y. R. Cheon, Y. J. Kim, J. Y. Back, T. K. An, C. E. Park, Y.-H. Kim, *J. Mater. Chem. A* **2014**, *2*, 16443; c) A. K. K. Kyaw, D. H. Wang, C. Luo, Y. Cao, T. -Q.Nguyen, G. C. Bazan, A. J. Heeger, *Adv. Energy Mater.* **2014**, *4*, 1301469; d) M. T. Dang, L. Hirsch, G. Wantz, J. D. Wuest, *Chem. Rev.* **2013**, *113*, 3734; e) A. Pivrikas, P. Stadler, H. Neugebauer, N. S. Sariciftci, *Org. Electron.* **2008**, *9*, 775.
[21] a) T. Xiao, H. Xu, G. Grancini, J. Mai, A. Petrozza, U.-S. Jeng, Y. Wang, X. Xin, Y. Lu, N. S. Choon, H. Xiao, B. S. Ong, X. Lu, N. Zhao, *Sci. Rep.* **2014**, *4*, 5211; b) J. A. Bartelt, Z. M. Beiley, E. T. Hoke, W. R. Mateker, J. D. Douglas, B. A. Collins, J. R. Tumbleston, K. R. Graham, A. Amassian, H. Ade, J. M. J. Frechet, M. F. Toney, M. D. McGehee, *Adv. Energy Mater.* **2013**, *3*, 364.
[22] a) Y. Liu, J. Zhao, Z. Li, C. Mu, W. Ma, H. Hu, K. Jiang, H. Lin, H. Ade, H. Yan, *Nat. Commun.* **2014**, *5*, 5293; b) J. R. Tumbleston, B. A. Collins, L. Yang, A. C. Stuart, E. Gann, W. Ma, W. You, H. Ade, *Nat. Photonics* **2014**, *8*, 385; c) I. Osaka, M. Saito, H. Mori, T. Koganezawa, K. Takimiya, *Adv. Mater.* **2012**, *24*, 425.
[23] a) Y. Sun, J. Seifter, M. Wang, L. A. Perez, C. Luo, G. C. Bazan, F. Huang, Y. Cao, A. J. Heeger, *Adv. Energy Mater.* **2014**, *4*, 1301601; b) E. Zhou, J. Cong, K. Hashimoto, K. Tajima, *Adv. Mater.* **2013**, *25*, 6991; c) C. Liu, X. Hu, C. Zhong, M. Huang, K. Wang, Z. Zhang, X. Gong, Y. Cao, A. J. Heeger, *Nanoscale* **2014**, *6*, 14297.
[24] T. Earmme, Y.-J. Hwang, N. M. Murari, S. Subramaniyan, S. A. Jenekhe, *J. Am. Chem. Soc.* **2013**, *135*, 14960.
[25] a) Z. Chen, P. Cai, J. Chen, X. Liu, L. Zhang, L. Lan, J. Peng, Y. Ma, Y. Cao, *Adv. Mater.* **2014**, *26*, 2586; b) Y. Li, P. Sonar, L. Murphy, W. Hong, *Energy Environ. Sci.* **2013**, *6*, 1684; c) Y. R. Cheon, Y. J. Kim, J. Ha, M.-J. Kim, C. E. Park, Y.-H. Kim, *Macromolecules* **2014**, *47*, 8570 .
[26] A. Pivrikas, N. S. Sariciftci, G. Juska, R. Osterbacka, *Prog. Photovolt: Res. Appl.* **2007**, *15*, 677.